Supplementary Information (SI) for Journal of Materials Chemistry A.

Supporting Information

Synergistic Sodium Storage in Bismuth-Loaded Polycellular Carbon Spheres: High Diffusion Kinetics and Stability

Jinhua Zhang[a], Yongfeng Li[a] *, Yanzhen Liu[b], Yu Cui[c], Xiangru Zhu[a], Xiaowen Zhang[a], Chunli Guo[c] *

[a] College of Artificial Intelligence, Taiyuan University of Technology, Taiyuan 030024, China

[b] CAS Key Laboratory of Carbon Materials, Institute of Coal Chemistry, Chinese Academy of Sciences, Taiyuan 030001, China

[c] College of Materials Science and Engineering, Taiyuan University of Technology, Taiyuan 030024, China

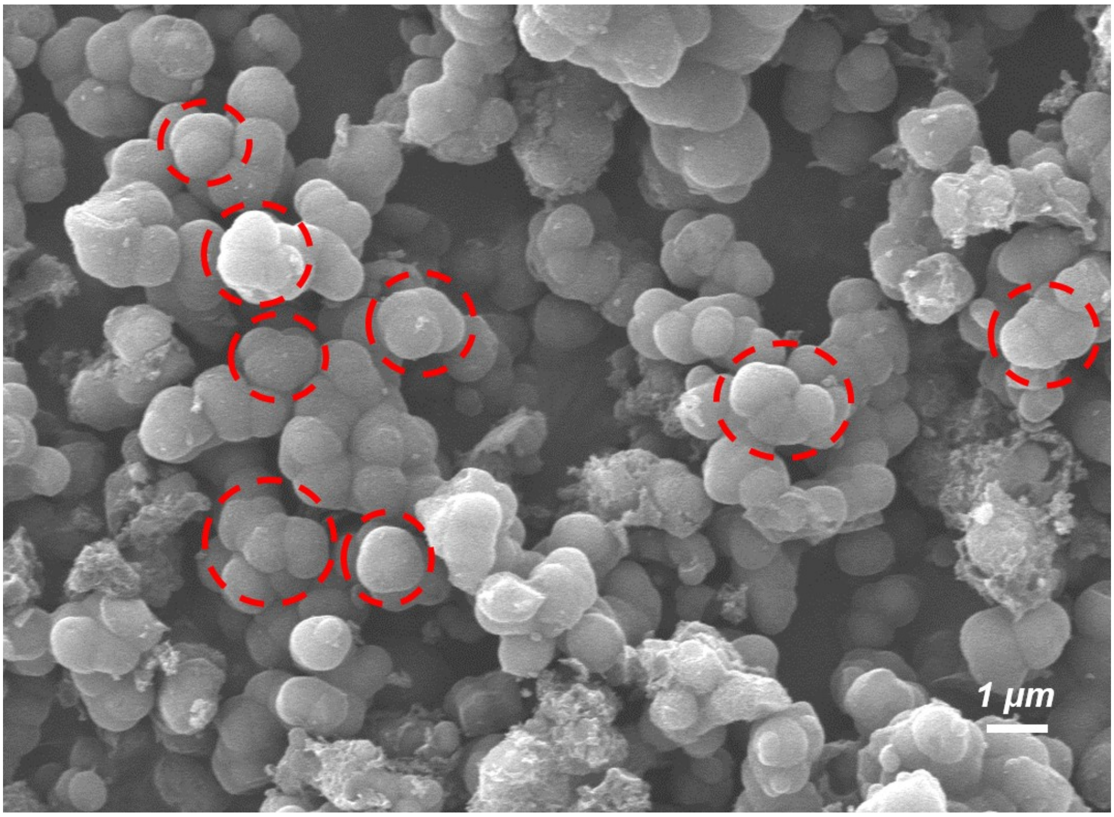

Fig. S1. SEM images of PCSs with bicellular or polycellular structures.

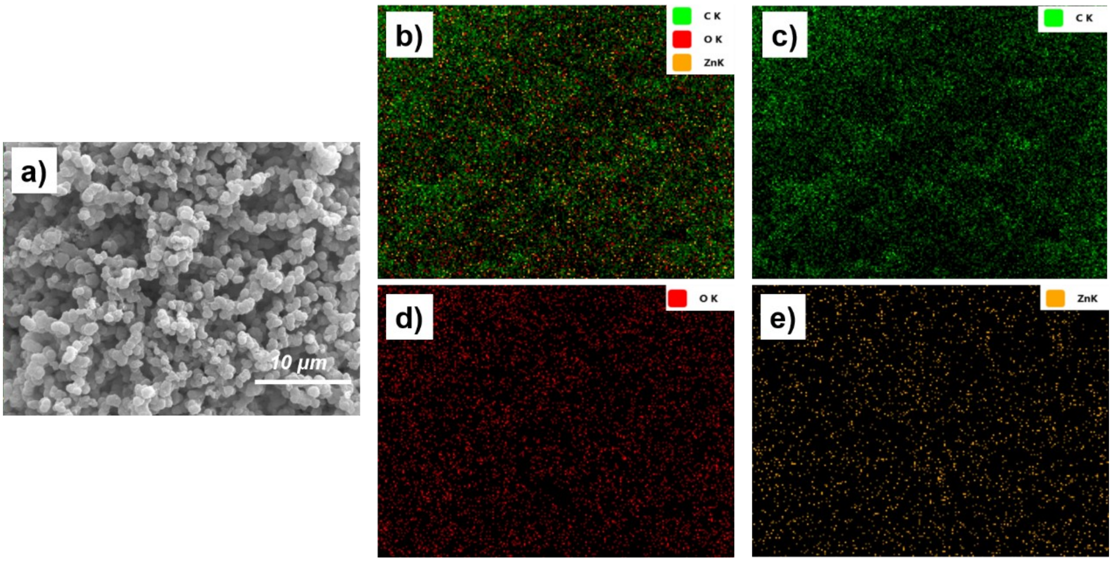

Fig. S2. (a) Scanning electron microscope images of the prepared PCSs. (b-e) Corresponding elemental maps.

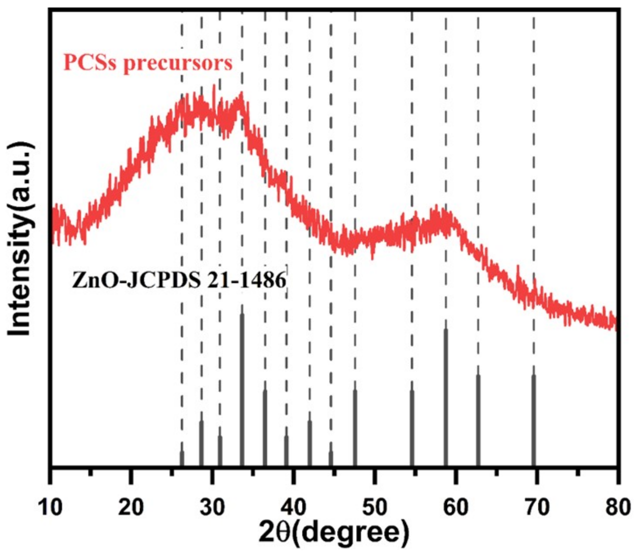

Fig. S3. XRD pattern of PCSs precursors.

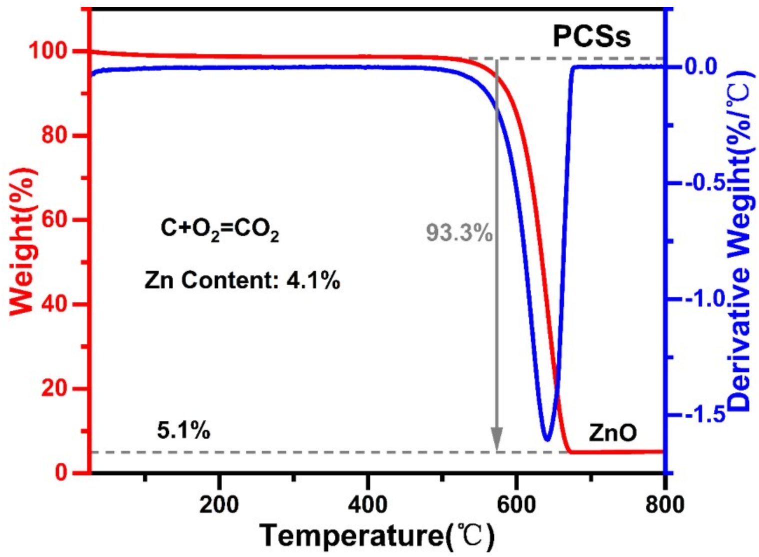

Fig. S4. Thermogravimetric and TGA curves of PCSs.

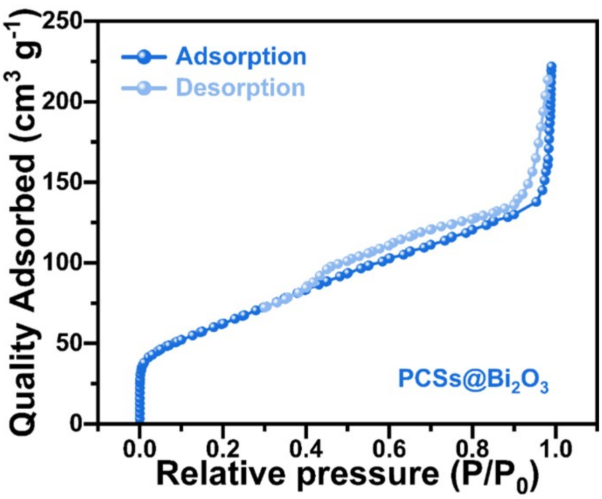

Fig. S5. N_2 adsorption/desorption isotherms of PCSs@Bi_2O_3.

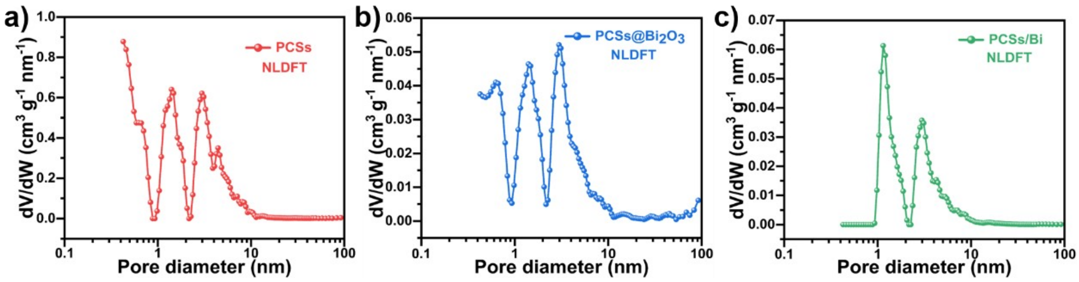

Fig. S6. (a, b, c) NLDFT full pore distribution of PCSs, PCSs@Bi_2O_3 and PCSs/Bi, respectively.

Table S1 Comparison of specific surface area, pore volume and average pore size of different samples

sample name	**S_{BET} (m^2 g^{-1})**	**V_p (cm^3 g^{-1})**	**average pore diameter (BJH) (nm)**
PCSs	2575.10	2.47	3.27
PCSs@Bi_2O_3	221.80	0.34	5.18
PCSs/Bi	132.20	0.13	3.38

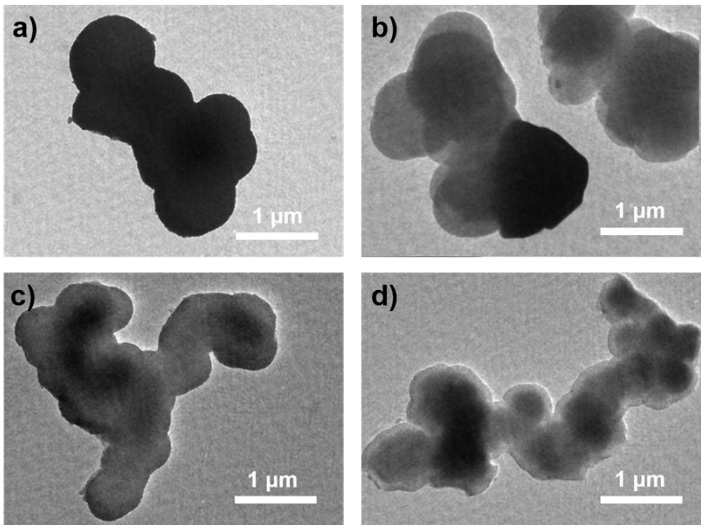

Fig. S7. (a) TEM image of PCSs precursor. (b, c, d) TEM image of PCSs precursors reacted at 800 °C for 2h, 900 °C for 2h and 900 °C for 4h, respectively.

Table S2 Mass of materials before and after annealing of PCSs precursors under different reaction conditions

Temperature (°C)	**Time (h)**	**Mass before annealing (g)**	**Mass after annealing (g)**
800	2	0.300	0.185
900	2	0.300	0.026
	4	0.300	0.025
1000	2	0.300	0.018
	4	0.300	≤ 0.010

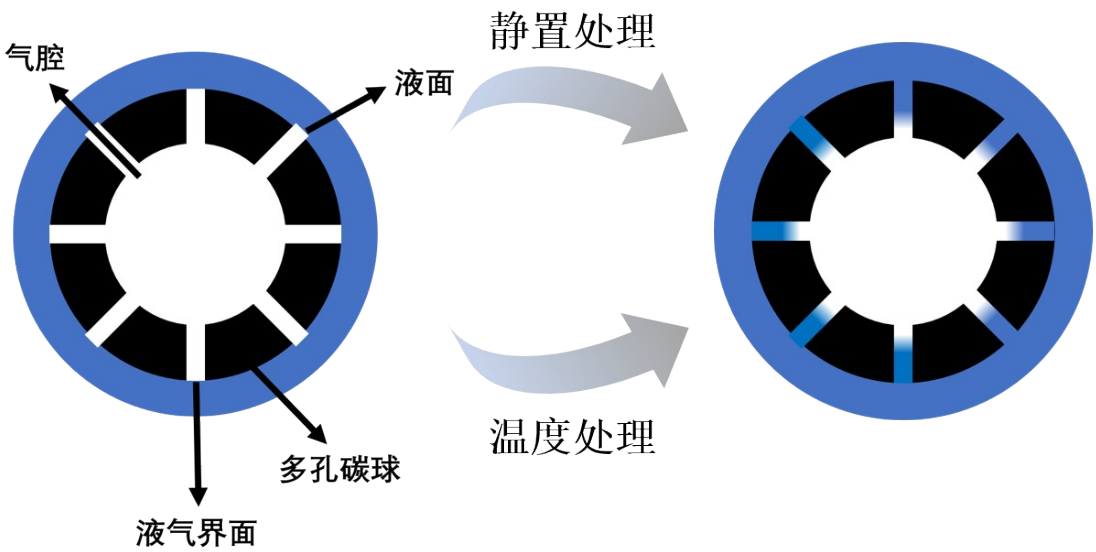

Fig. S8. Schematic representation of PCSs with improved wettability by temperature treatment and standing treatment.

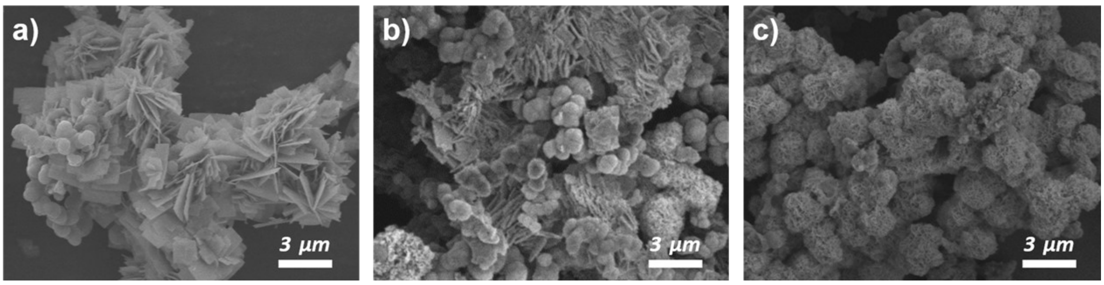

Fig. S9. (a) PCSs/Bi_2O_3 composites obtained without treatment. (b) PCSs/Bi_2O_3 composites obtained with ultrasonic treatment only. (c) PCSs@Bi_2O_3 composites obtained.

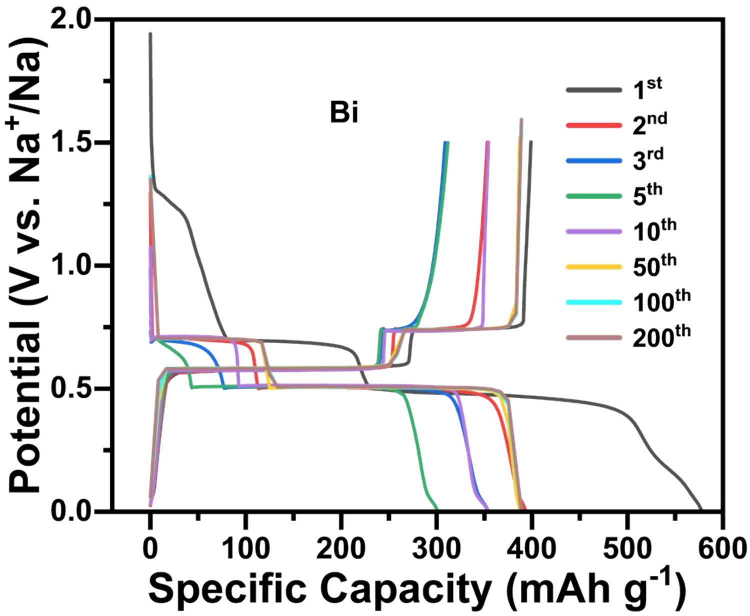

Fig. S10. GCD curves of Bi at a current density of 1 A g^{-1} for different cycles.

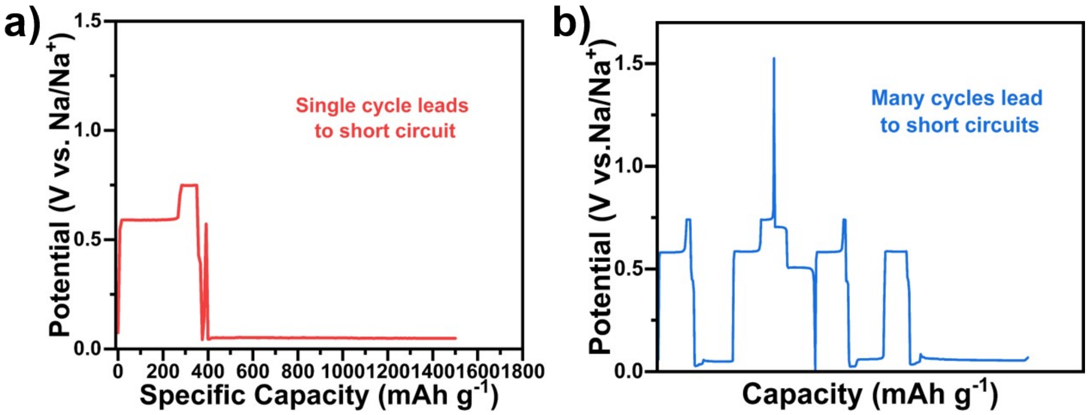

Fig. S11. (a) Charging curve with micro-short circuit up to complete short circuit in a single cycle. (b) Charging curves with several cycles of micro-short-circuits up to complete short-circuits.

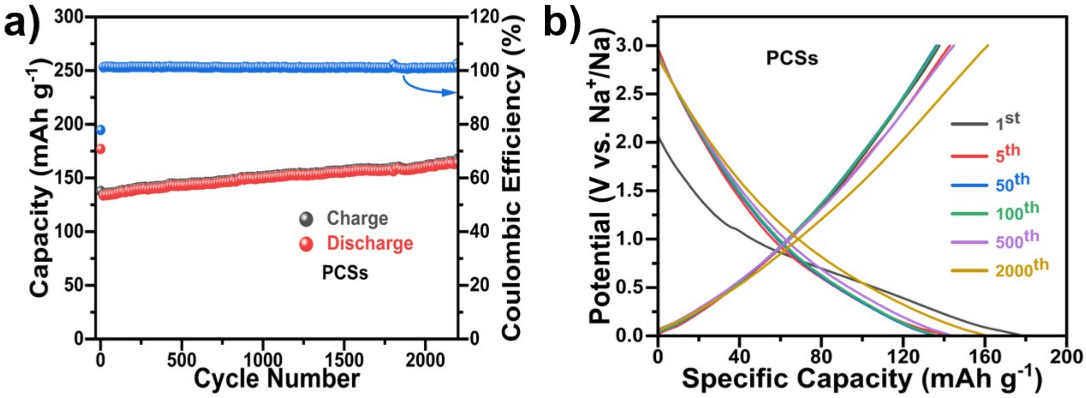

Fig. S12. (a) Long cycling curves of PCSs at 1 A g^{-1}. (b) GCD curves of PCSs at a current density of 1 A g^{-1} for different cycles.

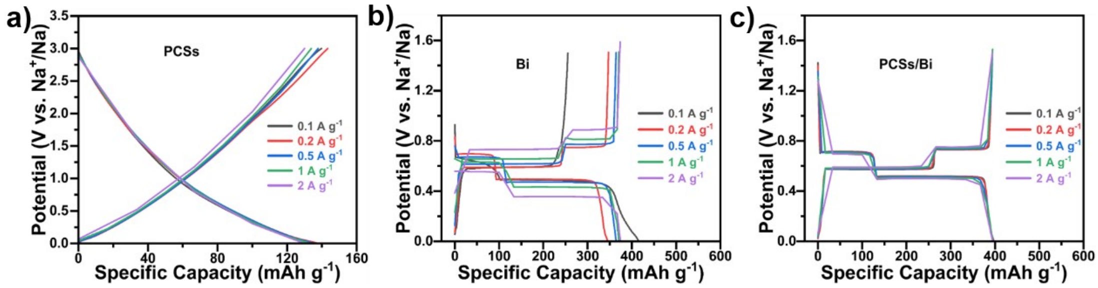

Fig. S13. Charge-discharge curves of (a) PCSs, (b) Bi and (c) PCSs/Bi at different current densities.

Table S3. Comparison of electrochemical properties of different materials in the literature

Sample	Cycling performance (mAh g^{-1})	Rate capability (mAh g^{-1})	Ref
PCSs/Bi	389 after 1500 cycles at 1 A g^{-1}	396.5 at 0.1 A g^{-1} 395.0 at 0.2 A g^{-1} 394.5 at 0.5 A g^{-1} 394.6 at 1 A g^{-1} 394.3 at 2 A g^{-1}	This work

		394.2 at 3 A g^{-1} 393.4 at 4 A g^{-1} 391.7 at 5 A g^{-1}	
Bi-NS@C	106 after 1000 cycles at 1 A g^{-1}	170 at 0.05 A g^{-1} 110 at 2 A g^{-1}	1
Bi@PDA	235 after 2000 cycles at 10 A g^{-1}	300 at 1 A g^{-1} 282 at 2 A g^{-1} 262 at 5 A g^{-1} 252 at 10 A g^{-1} 240 at 20 A g^{-1} 211 at 50 A g^{-1} 178 at 100 A g^{-1}	2
Bi@void@C	198 after 10000 cycles at 20 A g^{-1}	270 at 1 A g^{-1} 265 at 2 A g^{-1} 255 at 5 A g^{-1} 246 at 10 A g^{-1} 231 at 20 A g^{-1} 190 at 50 A g^{-1} 173 at 100 A g^{-1}	3
Bi@N-doped C	320 after 1000 cycles at 1 A g^{-1}	410 at 0.05 A g^{-1} 396 at 0.1 A g^{-1} 391 at 0.4 A g^{-1} 386 at 0.8 A g^{-1} 380 at 1.2 A g^{-1} 373 at 1.6 A g^{-1} 368 at 2 A g^{-1}	4
PBCNSs	373.4 after 2000 cycles at 0.5 A g^{-1}	400.3 at 0.2 A g^{-1} 385.6 at 0.4 A g^{-1} 380.6 at 0.8 A g^{-1} 378.5 at 2 A g^{-1} 378.2 at 4 A g^{-1} 377.9 at 8 A g^{-1} 377.0 at 15 A g^{-1} 374.9 at 20 A g^{-1} 372.8 at 25 A g^{-1}	5
Bi/C	310 after 100 cycles at 0.1 A g^{-1}	315 at 0.1 A g^{-1} 296 at 1 A g^{-1} 292 at 2 A g^{-1} 284 at 5 A g^{-1} 280 at 10 A g^{-1}	6
Bi@C@GR	300 after 80 cycles at 0.1 A g^{-1}	600 at 0.1 A g^{-1} 440 at 0.2 A g^{-1} 331 at 0.4 A g^{-1} 236 at 0.8 A g^{-1}	7

		175 at 1.6 A g^{-1}	
Ops-Bi/C	361 after 10000 cycles at 5 A g^{-1}	396 at 0.2 A g^{-1} 393 at 1 A g^{-1} 395 at 5 A g^{-1} 392 at 10 A g^{-1} 381 at 20 A g^{-1}	8
Bi@C	339 after 200 cycles at 0.2 A g^{-1}	331 at 0.1 A g^{-1} 343 at 0.3 A g^{-1} 343 at 0.5 A g^{-1} 341 at 1 A g^{-1} 338 at 2 A g^{-1} 327 at 5 A g^{-1}	9
Bi@NC	386.2 after 200 cycles at 0.2 A g^{-1}	392 at 0.1 A g^{-1} 376.7 at 0.2 A g^{-1} 363.9 at 0.5 A g^{-1} 359.5 at 1 A g^{-1} 347.5 at 2 A g^{-1} 344.1 at 5 A g^{-1} 338.2 at 10 A g^{-1}	10
Bi@MC	384 after 4800 cycles at 5 A g^{-1}	398 at 1.25 A g^{-1} 386 at 2.5 A g^{-1} 384 at 6.25 A g^{-1} 383 at 12.5 A g^{-1} 376 at 25 A g^{-1} 361 at 37.5 A g^{-1} 345 at 50 A g^{-1}	11
Bi@PVP	283 after 20000 cycles at 5 A g^{-1}	283 at 5 A g^{-1} 284 at 10 A g^{-1} 277 at 20 A g^{-1} 247 at 40 A g^{-1}	12
CMT@Bi-C	82.5 after 5000 cycles at 10 A g^{-1}	283 at 5 A g^{-1} 224 at 160 A g^{-1} 189 at 200 A g^{-1}	13
LC-Bi	301 after 2600 cycles at 1 A g^{-1}	372.0 at 0.1 A g^{-1} 354.4 at 0.5 A g^{-1} 349.4 at 1 A g^{-1} 346.6 at 2 A g^{-1} 345.1 at 5 A g^{-1} 343.8 at 10 A g^{-1} 342.8 at 20 A g^{-1} 337.9 at 50 A g^{-1} 333.4 at 100 A g^{-1}	14
P-Bi/C	278.1 after 500 cycles at 20 A g^{-1}	369.8 at 0.4 A g^{-1} 341.4 at 4 A g^{-1}	15

		327.6 at 12 A g^{-1} 307.5 at 20 A g^{-1} 274.4 at 32 A g^{-1}	
Bi@NC	—	384.8 at 0.1 A g^{-1} 376.1 at 0.2 A g^{-1} 362.4 at 0.5 A g^{-1} 354.8 at 1 A g^{-1} 351.9 at 2 A g^{-1} 349.3 at 5 A g^{-1} 341.5 at 10 A g^{-1}	16
Bi/MWCNTs	254 after 500 cycles at 1 A g^{-1}	300 at 1 A g^{-1} 292 at 2 A g^{-1} 285 at 5 A g^{-1} 272 at 10 A g^{-1} 245 at 20 A g^{-1}	17
Bi MF	338.6 after 1200 cycles at 1 A g^{-1}	359.7 at 1 A g^{-1} 358.9 at 5 A g^{-1} 357.5 at 10 A g^{-1} 353.9 at 20 A g^{-1} 350.0 at 30 A g^{-1} 343.4 at 40 A g^{-1} 338.9 at 50 A g^{-1}	18
Fbi@NC	378.3 after 600 cycles at 1 A g^{-1}	385.8 at 0.1 A g^{-1} 386.3 at 0.5 A g^{-1} 386.4 at 1 A g^{-1} 385.7 at 3 A g^{-1} 385.2 at 5 A g^{-1} 384.4 at 8 A g^{-1} 383.8 at 10 A g^{-1} 382.4 at 15 A g^{-1} 380.5 at 20 A g^{-1} 377.1 at 25 A g^{-1} 368.2 at 30 A g^{-1}	19
Bi@C-NSA	315.7 after 1500 cycles at 1 A g^{-1}	356.5 at 0.05 A g^{-1} 324.0 at 0.1 A g^{-1} 309.7 at 0.2 A g^{-1} 301.0 at 0.5 A g^{-1} 296.1 at 1 A g^{-1} 284.4 at 2 A g^{-1}	20
Bi@N-C	194.3 after 4000 cycles at 10 A g^{-1}	208 at 0.1 A g^{-1} 213.1 at 0.2 A g^{-1} 218.4 at 0.5 A g^{-1} 218.5 at 1 A g^{-1} 217.2 at 2 A g^{-1}	21

		212.3 at 5 A g^{-1} 206.5 at 10 A g^{-1} 199.1 at 20 A g^{-1} 191.1 at 50 A g^{-1} 152.2 at 100 A g^{-1} 119.5 at 150 A g^{-1} 110.0 at 200 A g^{-1}	
Bi@LNPC	325.4 after 4000 cycles at 1 A g^{-1}	351.5 at 20 A g^{-1} 342.8 at 50 A g^{-1}	22

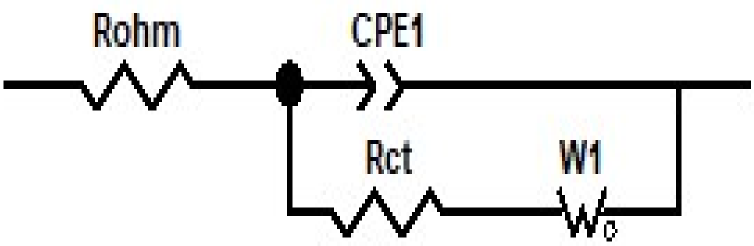

Fig. S14. Equivalent circuit diagram corresponding to the Nyquist curve.

Table S4. Fitted values of R_{ohm} and R_{ct} for different materials at different cycles

Electrode	Cycle	R_{ohm} (Ω)	R_{ct} (Ω)
YSCSs	Before cycling	1.195	2.865
	After 100 cycles	1.212	6.590
Bi	Before cycling	1.305	3.622
	After 100 cycles	1.165	0.445
YSCSs/Bi	Before cycling	1.315	1.615
	After 1 cycle	0.986	1.591
	After 10 cycles	1.021	0.410
	After 50 cycles	1.031	0.394
	After 100 cycles	1.036	0.418

References

1. J. X. Qiu; S. Li; X. T. Su; Y. Z. Wang; L. Xu; S. Q. Yuan; H. M. Li; S. Q. Zhang, *Chem. Eng. J.* 2017, **320**, 300-307.

2. H. Yang; R. Xu; Y. Yao; S. Ye; X. Zhou; Y. Yu, *Adv. Funct. Mater.* 2019, **29**, 1809195.

2. H. Yang; L.-W. Chen; F. He; J. Zhang; Y. Feng; L. Zhao; B. Wang; L. He; Q. Zhang; Y. Yu, *Nano Lett.* 2019, **20**, 758-767.

4. P. Xue; N. N. Wang; Z. W. Fang; Z. X. Lu; X. Xu; L. Wang; Y. Du; X. C. Ren; Z. C. Bai; S. X. Dou; G. H. Yu, *Nano Lett.* 2019, **19**, 1998-2004.

5. J. H. Zhu; J. W. Wang; G. W. Li; L. Huang; M. Y. Cao; Y. P. Wu, *J. Mater. Chem. A* 2020, **8**, 25746-25755.

6. H. Yuan; F. Ma; X. Wei; J. L. Lan; Y. Liu; Y. Yu; X. Yang; H. S. Park, *Adv. Energy Mater.* 2020, **10**, 2001418.

7. F. Zhang; X. Liu; B. Wang; G. Wang; H. Wang, *ACS Appl. Mater.* 2021**, 13**, 59867-59881.

8. Y. Li; X. Zhong; X. W. Wu; M. Q. Li; W. Zhang; D. Wang, *J. Mater. Chem. A* 2021, **9**, 22364-22372.

9. L. Liu; S. Li; L. Hu; X. Liang; W. Yang; X. Yang; K. Hu; C. Hou; Y. Han; S. Chou, *Carbon Energy* 2024, **6**.

10. L. Chen; X. He; H. Chen; S. Huang; M. Wei, *J. Mater. Chem. A* 2021, **9**, 22048-22055.

11. J. Chen; J. Xiao; J. Y. Li; H. Gao; X. Guo; H. Liu; G. X. Wang, *J. Mater. Chem. A* 2022, **10**, 20635-20645.

12. X. Zhong; Y. W. Chen; W. Zhang; Z. W. Zhang; M. Q. Li, *ACS Sustainable Chem. Eng.* 2022, **10**, 8856-8862.

13. B. Park; S. Lee; D.-Y. Han; H. Jang; D. Gi Seong; J.-K. Yoo; S. Park; Y. Oh; J. Ryu, *Appl. Surf. Sci.* 2023, **614**, 156188.

14. X. Zhang; X. Qiu; J. Lin; Z. Lin; S. Sun; J. Yin; H. N. Alshareef; W. Zhang, *Small* 2023, **19**, 2302071.

15. S. G. Guo; C. H. Wei; L. Wang; S. X. Mei; B. Xiang; Y. Zheng; X. M. Zhang; M. Javanbakht; B. Gao; P. K. Chu; K. F. Huo, *Cell Rep. Phys. Sci.* 2023, **4**, 101463.

16. S. Wei; W. Li; Z. Ma; X. Deng; Y. Li; X. Wang, *Small* 2023, **19**, 2304265.

17. J. Yu; D. Zhao; C. S. Ma; L. Feng; Y. H. Zhang; L. F. Zhang; Y. Liu; S. W. Guo, *J. Colloid Interface Sci.* 2023, **643**, 409-419.

18. J. Bai; Y. Liu; B. Pu; Q. Tang; Y. B. Wang; R. H. Yuan; J. Cui; Y. Yang; X. J. Zheng; B. Zhou; W. Q. Yang, *J. Mater. Chem. A* 2024, **12**, 11691-11700.

19. Z. Chen; X. Wu; Z. Sun; J. Pan; J. Han; Y. Wang; H. Liu; Y. Shen; J. Li; D. L. Peng; Q. Zhang, *Adv. Energy Mater.* 2024, **14**, 2400132.

20. Y. Wang; X. Xu; Y. Wu; F. Li; W. Fan; Y. Wu; S. Ji; J. Zhao; J. Liu; Y. Huo, *Adv. Energy Mater.* 2024, **14**, 2401833.

21. Q. Yao; C. Zheng; K. Liu; M. Wang; J. Song; L. Cui; D. Huang; N. Wang; S. X. Dou; Z. Bai; J. Yang, *Adv. Sci.* 2024, **11**, 2401730.

22. Z. H. Lin; X. Q. Qiu; X. H. Zu; X. S. Zhang; L. Zhong; S. R. Sun; S. H. Hao; Y. J. Sun; W. L. Zhang, *Rare Met.* 2023, **43**, 1037-1047.